# 1 Strong Lensing

*Authors: Simon Huber*[1]*, Sherry H. Suyu*[2]*, Tanja Petrushevska*[3]

## 1.1 Supernovae Lensed by Galaxies

*Contributors: Simon Huber, Sherry H. Suyu*

The goal of this section is to evaluate how well we can measure time delays in strongly lensed SNe Ia (LSNe Ia), which yields with lens mass modeling a direct method to measure the Hubble constant.

To simulate observations randomly, we have used mock LSNe Ia from the OM 10 catalog [Oguri and Marshall, 2010], and produced the light curves for the mock SNe images with the spherically symmetric SN Ia W7 model [Nomoto et al., 1984] calculated with ARTIS (Applied Radiative Transfer In Supernovae) [Kromer and Sim, 2009] in combination with magnifications maps from GERLUMPH [Vernardos et al., 2015] to include the effect of microlensing similar as in [Goldstein et al., 2017]. To simulate data points for the light curves, we place the mock system randomly in one of 10 chosen fields in the WFD (wide fast deep survey), where we follow the observation pattern from 18 different cadence strategies. From this we get simulated observations, where the error is calculated according to [LSST Science Collaboration et al., 2009, sec 3.5, p. 67]. To evaluate the mock data and get a measured time delay we use the free knot spline optimizer from PyCS (Python Curve Shifting) [Tewes et al., 2013, Bonvin et al., 2016]. Details of this work will be presented in Huber et al. (in preparation).

We have investigated two different metrics, first using LSST data only to measure time delays and second, using LSST as a discovering machine in combination with follow-up observations to measure delays. We assume follow-up observations would start 2 days after the third LSST data point in any filter exceeds the 5-$\sigma$ depth, where the follow-up is done in 3 filters (g,r,i) every second night.

To have sufficient statistics, we investigate for each cadence strategy 202 mock LSNe Ia for "LSST only", and 100 mock systems for "LSST + follow up". For each of the mock systems we draw 100 random starting configurations. A starting configuration corresponds to a random position in the microlensing map and a random field from the 10 chosen fields, where it is placed randomly in one of the observing seasons such that the detection requirement from OM 10 is fulfilled. For each of these starting configurations we then draw 1000 different noise realizations of light curves. For each realization we calculate the deviation from the true time delay as

$$\tau_{\mathrm{d}} = \frac{t_{\mathrm{measured}} - t_{\mathrm{true}}}{t_{\mathrm{true}}}. \tag{1.1}$$

For one strategy and double LSNe Ia, we have thus 1(delay for the one pair of images) $\times$ 6(filters) $\times$ 100(starting configurations) $\times$ 1000(noise realisations) time-delay deviations as in (1.1). For the 6 pairs of images for a quad system we have a sample of $6 \times 6 \times 100 \times 1000$. The resulting distribution of time-delay deviation is investigated for each pair of images and each filter separately. From the $100 \times 1000$ time-delay deviations we define accuracy as the median $\tau_{\mathrm{d},50}$ and precision as $\delta = (\tau_{\mathrm{d},84} - \tau_{\mathrm{d},16})/2$, where $\tau_{\mathrm{d},84}$ is the 84th and $\tau_{\mathrm{d},16}$ the 16th percentile. Measuring $H_0$ with 1% accuracy requires that the accuracy in the delay deviation $\tau_{\mathrm{d},50}$ is $< 1\%$ (since $H_0 \propto t_{\mathrm{true}}^{-1}$). Since the 6 time-delay deviations from the 6 filters are independent we combine them into a single time-delay deviation via the weighted mean. This means that in the end we have for one strategy and a mock LSNe Ia one

$$\tau_{\mathrm{d},50} \pm \delta \tag{1.2}$$

per pair of images.

From this we summarize the results and quantify the 18 investigated cadences. Given that $H_0 \propto \frac{1}{t}$, where $t$ is the time delay between two images, we aim for accuracy ($\tau_{\mathrm{d},50}$) smaller than 1 percent and precision ($\delta$) smaller than 5 percent in equation 1.2. The accuracy requirement is needed for measuring $H_0$ with 1% uncertainty, and the precision requirement ensures that the delay uncertainty does not dominate the overall uncertainty on $H_0$ given typical mass modeling uncertainties of $\sim 5\%$

[1] shuber@mpa-garching.mpg.de
[2] suyu@mpa-garching.mpg.de
[3] tanja.petrushevska@ung.si

[e.g., Suyu et al., 2018]. A quad system is counted as successful if one of the 6 delays fulfills this requirement.

From this investigation we get the fraction of systems with successful measured delays. These numbers have to be combined with the total number of LSNe Ia we expect to detect for different strategies. We approximate the total number of LSNe Ia as

$$N_{\mathrm{LSNeIa,cad}} = N_{\mathrm{LSNeIa,OM10}} \frac{\Omega_{\mathrm{cad}}}{\Omega_{\mathrm{OM10}}} \frac{\bar{t}_{\mathrm{eff,cad}}}{t_{\mathrm{eff,OM10}}} \tag{1.3}$$

where $N_{\mathrm{LSNeIa,OM10}} = 45.7$, $\Omega_{\mathrm{OM10}} = 20\,000\,\mathrm{deg}^2$ and $t_{\mathrm{eff,OM10}} = 2.5\,\mathrm{yr}$ from Oguri and Marshall [2010]. $\Omega_{\mathrm{cad}}$ is the survey area for a given cadence. We assume $\Omega_{\mathrm{cad}} = 24\,700\,\mathrm{deg}^2$ for pontus_2002, kraken_2044, mothra_2049 and nexus_2097, and for the other strategies $\Omega_{\mathrm{cad}} = 18\,000\,\mathrm{deg}^2$. $\bar{t}_{\mathrm{eff,cad}}$ is the cumulative seasonal length for a given cadence, where we have averaged over all LSST fields where observations are taken.

Combining the fraction of systems with the total number of LSNe Ia we get the number of LSNe Ia over the 10 year survey, where the delay can be measured with accuracy $< 1$ % and precision $< 5$ % . The results are shown in figure 1.

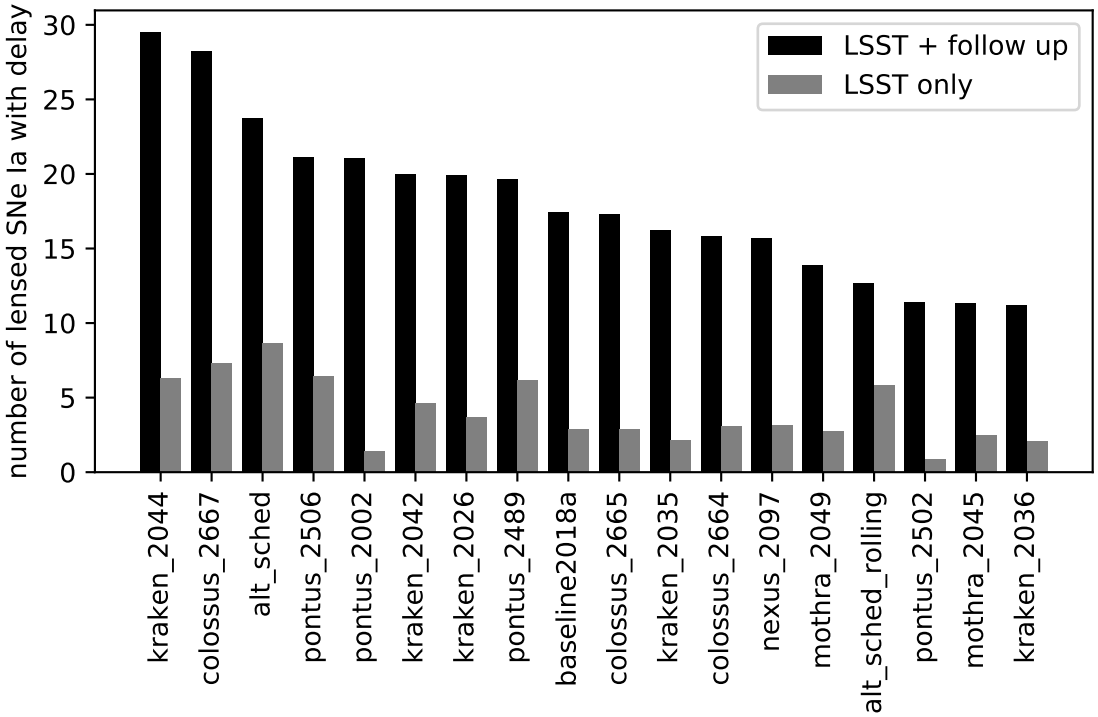


Figure 1: This plot quantifies 18 different cadence strategies for measuring time delays in LSNe Ia. The black bars consider LSST as a discovery machine in combination with follow-up observations in 3 filters (g,r,i) every second night. We assume follow-up observation would start 2 days after the third LSST data point in any filter exceeding the 5-$\sigma$ depth. For the grey bars only LSST data is used to measure time delays. Since for LSST only, the total numbers with good delays are very low, we advocate using LSST as a discovering machine with observational follow up. Therefore the black bars are the relevant ones to quantify different cadences. To summarize we are perfectly fine with a "baseline2018a" like cadence. To improve on this cadence longer cumulative seasonal lengths $\bar{t}_{\mathrm{eff,cad}}$, bigger survey areas $\Omega_{\mathrm{cad}}$ and a better sampling are helpful. On the other hand, rolling cadences are clearly disfavored despite the better sampling due to the substantially shortened cumulative seasonal length.

For the metric LSST data only we see that for the best strategies we will just have a few systems where time-delay measurements are possible. Follow-up observations are therefore necessary to increase the number of LSNe Ia with delays as visible which makes LSST + follow up the important metric to rank different observing strategies.

To summarize, for our science case of measuring time delays from as many lensed SNe as possible, it would be more effective to use LSST as a discovering machine with additional follow-up, instead of relying on LSST completely for the delay measurements. Therefore we are fine with the current baseline cadence. To improve on this cadence longer cumulative seasonal lengths $\bar{t}_{\rm eff,cad}$, bigger survey areas $\Omega_{\rm cad}$ and a more frequent sampling are helpful. The most important result from our investigation is that rolling cadences are clearly disfavored, because their shortened cumulative season lengths $\bar{t}_{\rm eff,cad}$ lead to overall a more negative impact on the number of LSNe Ia with delays, compared to the gain from the increased sampling frequency.

Further Goldstein et al. [2018] performed detailed simulations of the gLSN population using a completely independent technique and pipeline and reached similar conclusions to the ones presented here: rolling cadences are strongly disfavored, and wide-area, long-season surveys with well sampled light curves are optimal.

## 1.2 Supernovae Lensed by Galaxy Clusters

*Contributors: Tanja Petrushevska*

Here, we focus on prospects of observing supernovae which are lensed by known galaxy clusters. High-z galaxies that appear as multiple images in the cluster field can host supernova explosions. Strongly lensed supernovae by galaxy clusters not only can be used as tools to examine both global cosmology, but also the local environment of the cluster lenses. Cluster lensing time scales are typically much longer and the microlensing effects are almost negligible, which makes their measurement potentially more feasible, especially if the lens potential is well studied and the predicted time delays have small uncertainties. We calculate the expected number of supernovae Ia in the multiply lensed background galaxies by using the Hubble Frontier Fields cluster and Abell 1689. These clusters have been extensively studied, and given the good quality data, well constrained magnification maps and time delays can be obtained from the lensing models. We only considered those that have a spectroscopic redshift. To obtain better image depth, we combine the images that are taken closer than 5 days in time. We note that these are a lower limits, since we have only considered few clusters and the galaxies with spectroscopic redshift. For this science case, the most important bands are i, z and y. Since most of the light of nearby SNe is in the optical bands, these filters are optimal for finding high-z SNe, as their light is redshifted to the longer wavelengths. When we consider the different observing strategies, we find that the rolling cadences (mothra_2045 and pontus_2502) are disfavored given that they do not return to the clusters as the other observing strategies. The strategy pontus_2489 provides slightly better prospects compared to the others because it provides the most number of visits to the same cluster fields.

## 1.3 Lensed Quasars

*Contributors: TBD*

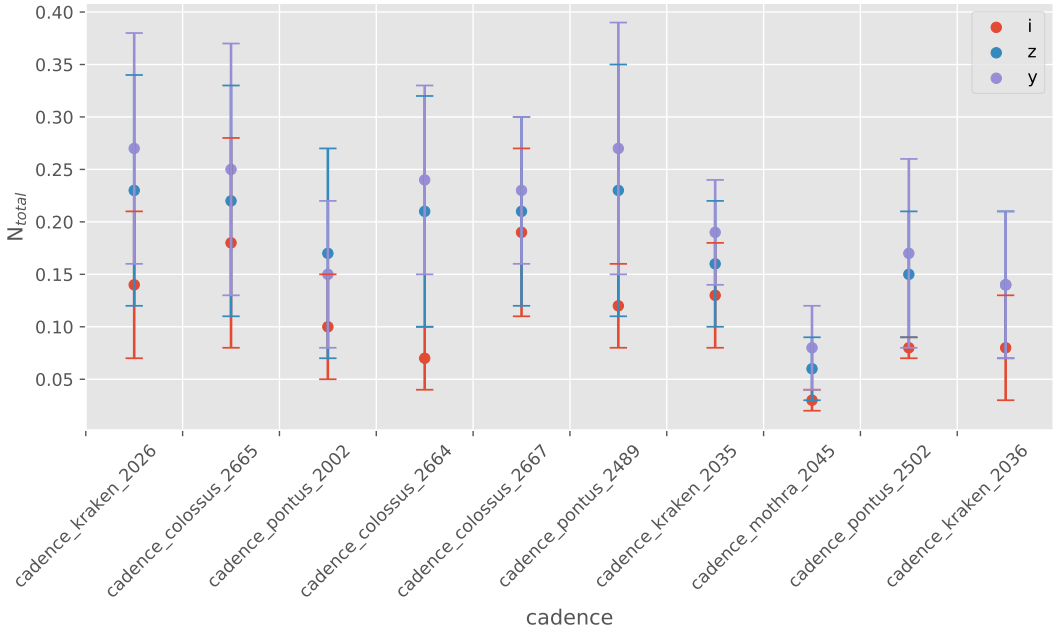


Figure 2: The expected total number of strongly lensed SNe Ia arising from the multiply imaged galaxies in the Hubble Frontier Fields and Abell 1689 in function of the observing strategy. **TODO (Tanja): include new cadences and do same estimates for CC SNe***

# References


M. Oguri and P. J. Marshall. Gravitationally lensed quasars and supernovae in future wide-field optical imaging surveys. *MNRAS*, 405:2579–2593, July 2010. doi: 10.1111/j.1365-2966.2010.16639.x.

K. Nomoto, F.-K. Thielemann, and K. Yokoi. Accreting white dwarf models of Type I supernovae. III - Carbon deflagration supernovae. *apj*, 286:644–658, November 1984. doi: 10.1086/162639.

M. Kromer and Sim. Time-dependent three-dimensional spectrum synthesis for Type Ia supernovae. *MNRAS*, 398:1809–1826, 2009. doi: 10.1111/j.1365-2966.2009.15256.x.

Georgios Vernardos, Christopher J. Fluke, Nicholas F. Bate, Darren Croton, and Dany Vohl. GERLUMPH Data Release 2: 2.5 billion simulated microlensing light curves. *Astrophys. J. Suppl.*, 217 (2):23, 2015. doi: 10.1088/0067-0049/217/2/23.

Daniel A. Goldstein, Peter E. Nugent, Daniel N. Kasen, and Thomas E. Collett. Precise Time Delays from Chromatically Microlensed Type Ia Supernovae. 2017.

LSST Science Collaboration, P. A. Abell, J. Allison, S. F. Anderson, J. R. Andrew, J. R. P. Angel, L. Armus, D. Arnett, S. J. Asztalos, T. S. Axelrod, and et al. LSST Science Book, Version 2.0. *ArXiv e-prints*, December 2009.

M. Tewes, F. Courbin, and G. Meylan. COSMOGRAIL: the COSmological MOnitoring of GRAvItational Lenses. XI. Techniques for time delay measurement in presence of microlensing. *aap*, 553: A120, May 2013. doi: 10.1051/0004-6361/201220123.

V. Bonvin, M. Tewes, F. Courbin, T. Kuntzer, D. Sluse, and G. Meylan. COSMOGRAIL: the COSmological MOnitoring of GRAvItational Lenses XV. Assessing the achievability and precision of time-delay measurements. *Astron. Astrophys.*, 585:A88, 2016. doi: 10.1051/0004-6361/201526704.

R. Kormann, P. Schneider, and M. Bartelmann. Isothermal elliptical gravitational lens models. *AAP*, 284:285–299, April 1994.

S. H. Suyu, T.-C. Chang, F. Courbin, and T. Okumura. Cosmological Distance Indicators. *Space Science Reviews*, 214:91, August 2018. doi: 10.1007/s11214-018-0524-3.

Daniel A. Goldstein, Peter E. Nugent, and Ariel Goobar. Rates and Properties of Strongly Gravitationally Lensed Supernovae and their Host Galaxies in Time-Domain Imaging Surveys. 2018.